J Biomol NMR (2007) 38:255–266
DOI 10.1007/s10858-007-9164-8

ARTICLE

Vibrational averaging of chemical shift anisotropies in model peptides

Sishi Tang · David A. Case

Received: 11 April 2007 / Accepted: 14 May 2007 / Published online: 12 June 2007

Abstract The effects of chemical shift anisotropy (CSA) are evident in line-shapes or side-band analysis in solid-state NMR, in the observed line positions in partially oriented samples, and in relaxation effects in liquid-state studies. In all of these cases, the effective shielding tensor is influenced by fast vibrational averaging in addition to larger-amplitude internal motions and to overall libration or rotation. Here we compute the contributions of vibrational averaging (including zero-point motions) to the CSA relaxation strengths for the nitrogen and carbonyl carbon in two simple peptide models, and for snapshots taken from a path-integral simulation of a small protein. Because the ^{15}N shielding tensor is determined by all the atoms of the peptide group, it is less influenced by vibrational motion than (for example) the N–H dipolar interaction, which is more sensitive to the motion of the light hydrogen atom. Computed order parameters for CSA averaging are hence much closer to unity than are N–H dipolar order parameters. This leads to a reduction by about 9% in the magnitude of the amide nitrogen CSA that is needed to fit liquid-state relaxation data. Similar considerations apply to the carbonyl carbon shielding tensor, but in this case the differences between dipolar and CSA averaging are smaller. These considerations will be important for making comparisons between CSA tensors extracted from various NMR experiments, and for comparisons to quantum chemical calculations carried out on static conformers.

Keywords Chemical shift · Peptide · Vibrations

S. Tang · D. A. Case (✉)
Department of Molecular Biology, The Scripps Research Institute, La Jolla, CA 92037, USA
e-mail: case@scripps.edu

Introduction

Chemical shielding is a tensor quantity, and the effective field at the nucleus depends upon the orientation of this tensor with respect to the magnetic field. The way in which this orientation is averaged can provide important information about macromolecular structure and dynamics. This averaging affects line-shapes in solid state NMR, residual chemical shifts in partially aligned samples, and relaxation behavior in all environments. The basic theory of how motions affect the observed parameters is formally analogous to that used for dipolar coupling (Abragam 1961), but things are more complicated in practice, since shielding is an electronic property that (unlike dipolar couplings) can depend in a very complex way on nuclear coordinates. The way in which isotropic shifts are averaged by vibrational motion has been well investigated (Nielsen et al. 2000; Woodford and Harbison 2006), but much less is known about CSA effects. Here we use quantum chemical calculations and normal mode theory to study vibrational averaging in model peptides, in a manner analogous to that used previously to examine dipolar couplings (Case 1999). We also extract snapshots from a path-integral simulation of a small protein to compare with the simple peptide models.

Many standard treatments of relaxation theory implicitly assume that the principal components and directions of the CSA tensor are fixed in a local molecular frame, making the theory analogous to that used for dipolar couplings when bond distances and angles are assumed to be constant. This approach takes advantage of the fact that local vibrational averaging is invariably in the extreme narrowing limit, so that one can account for it through the use of an *effective* CSA tensor (or an effective bond length in the case of dipolar couplings). Since the components of the

CSA tensor are (in practice) almost always treated as empirical parameters, using such an effective tensor as a fitting parameter makes good sense. Nevertheless, there are a number of reasons why it would be useful to understand the details of the vibrational averaging that creates the effective tensors. First, different experiments involve different sorts of averaging: qualitatively, ''pure'' CSA relaxation experiments depend upon the square of the shielding tensor, whereas CSA/dipole cross-correlation, residual shifts and lineshapes in solid-state experiments involve terms linear in the shielding anisotropy. One needs a model for vibrational motion and its effects on shielding in order to compare results, or to fit multiple data sets to a single atomic model. Second, electronic structure calculations typically consider only static (average) structures. If insight from quantum chemistry is to become quantitatively useful for the interpretation of NMR data, we need to understand how to connect static and vibrationally-averaged shielding tensors.

The classic treatment of effects of vibrational averaging on dipolar and quadrupolar coupling is that of Henry and Szabo (Henry and Szabo 1985). The dipolar interaction depends only upon nuclear positions, so that its behavior under vibrational averaging is straightforward, assuming that vibrational normal modes are available. Quadrupolar relaxation depends upon the behavior of the electric field gradient (EFG) tensor, which is an electronic property; Henry and Szabo were able to make progress here by using a model in which the EFG was assumed to depend in a certain way upon bond length (and not upon any other geometric variables). Averaging of CSA interactions is a more complex problem since the dependence of shielding on molecular geometry is not well understood. Recently, Zuiderweg and co-workers have used density functional calculations to create a model for how carbonyl carbon CSA tensors in peptides depend upon the local nuclear geometry (Jordan et al. 2007). Using this, they could average over vibrational motion to obtain an effective tensor, *i.e.*, one that would show the same CSA relaxation in a rigid molecule as the real tensor does when vibrational effects are included. Here we use a simpler but more ''brute force'' approach, generating snapshots that sample local vibrational motion, and carrying out quantum chemistry calculations on each such snapshot. This eliminates the need to identify the most important geometric variables and to provide a fit for the complex behavior that connects CSA tensors and geometries; on the other hand, it means that each new type of averaging requires a fresh set of quantum calculations. As noted below, the two sorts of calculations give nearly identical conclusions for carbonyl carbons.

Theory

Relaxation theory

The general theory of NMR relaxation is covered in many places, and will not be repeated here (Kowalewski and Mäler 2006; Cavanagh et al. 2007). Under appropriate conditions, the influence of molecular motion on spin transition rates is governed by components of a spectral density function, $j_m^{\lambda,\lambda'}(\omega)$, which is the Fourier transform of a time-correlation function:

$$C_m^{\lambda,\lambda'}(\tau) = \left\langle \omega^{\lambda}(0)\omega^{\lambda'}(\tau)C_{2m}^{*}(\mathbf{u}^{\lambda}(0))C_{2m}(\mathbf{u}^{\lambda'}(\tau))\right\rangle \qquad (1)$$

Here λ and λ' denote the relaxation operators involved; we will be concerned here with dipolar relaxation, where $\omega^{\lambda} = \gamma_i\gamma_j/hr^3$, and CSA relaxation, where $\omega^{\lambda} = \gamma_i B\Delta\sigma$. Here the γ factors are nuclear magnetogyric ratios, r is the instantaneous distance between the spins whose dipolar coupling is being considered, B is the magnitude of the external magnetic field, and $\Delta\sigma$ is the instantaneous value of the shielding anisotropy. For dipolar coupling, the unit vector $\mathbf{u}^{\lambda}$ lies along the vector connecting the two spins, whereas for CSA effects, it is the direction of unique principal component of the shielding tensor. The brackets in Eq. 1 indicate an average over all the molecules in the ensemble, and $C_{2m} \equiv (4\pi/5)^{1/2}Y_{2m}$ is a modified spherical harmonic.

If there is no preferred direction in space, as in isotropic solution or in a randomly-oriented powder, the expression in Eq. 1 is independent of the subscript m, and we can average over the five possible values using the spherical harmonic addition theorem. This gives

$$C^{\lambda,\lambda'}(\tau) = \left\langle \omega^{\lambda}(0)\omega^{\lambda'}(\tau)P_2[\mathbf{u}^{\lambda}(0)\cdot\mathbf{u}^{\lambda'}(\tau)]\right\rangle \qquad (2)$$

where $P_2(x) \equiv (3x^2 - 1)/2$ is a Legendre polynomial. For local vibrational relaxation, the decay of these correlation functions is in the sub-picosecond regime, and we are always in the extreme narrowing limit for NMR relaxation. This implies that we can set τ to a value short compared to overall tumbling, and yet still large enough that the vectors at time τ have become uncorrelated with their values at time 0. Then Eq. 1 becomes

$$C_m^{\lambda,\lambda'}(\tau \to \infty) = \left\langle \omega^{\lambda}C_{2m}^{*}(\mathbf{u}^{\lambda})\right\rangle\left\langle \omega^{\lambda'}C_{2m}(\mathbf{u}^{\lambda'})\right\rangle \qquad (3)$$

where each average is over the equilibrium ensemble.

Since vibrational averaging takes place on a very rapid time scale, and has a small amplitude, we can effectively separate its correlation function from much slower processes such as overall rotational tumbling. In the Lipari-Szabo, or

''model-free'' approach (Lipari and Szabo 1982), the spectral density for the combination of fast internal and slower overall rotation becomes:

$$J^{LS} = \frac{2S^2\tau_c}{1+\omega^2\tau_c^2} + \frac{2(1-S^2)\tau}{1+\omega^2\tau^2} \tag{4}$$

Here, we have assumed for simplicity that the overall motion is isotropic with a rotational relaxation time τ_c. The squared order parameter, S^2 represents the plateau value of Eq. 3 (where $C^{\lambda\lambda'}$ is normalized to unity at time zero), and $\tau^{-1} = \tau_c^{-1} + \tau_e^{-1}$, where τ_e is the decay time for the internal motion. When $\tau_e = \tau_c$, as is the case here, the second term of Eq. 4 can be neglected; then the effect of the rapid vibrational motion is just to scale the rotational spectral density by a factor of S^2. The purpose of this paper is to provide some estimates of these scaling factors for plausible models of vibrational motion in peptides.

Vibrational averaging also affects solid-state NMR spectra, including powder patterns (or the closely allied spinning side-band analysis) that have traditionally provided our primary knowledge about chemical shielding anisotropies. Vibrational effects on solid-state lineshapes have been considered in detail before (Torchia and Szabo 1982; Henry and Szabo 1985; Ishii et al. 1997), and we will not repeat this analysis here. The general result is that the vibrationally averaged interaction strength extracted from a powder pattern is the square root of the interaction defined in Eq. 2 (assuming identical vibrations in the solid and liquid states). This is just what one might expect from the fact that the interaction Hamiltonian appears to second order in relaxation analysis, but only to first order in lineshape analysis. The same sort of square root relationship also holds for motional effects on residual dipolar couplings, for example (Tjandra and Bax 1997; Tsui et al. 2000). This simple connection between motionally averaged frequencies and relaxation depends on an assumption of axial symmetry (Henry and Szabo 1985; Tsui et al. 2000), but is approximately true even for non-axial systems.

The dipolar interaction tensor is always axially symmetric about the (instantaneous) bond vector, so that the $\mathbf{u}^\lambda$ direction in Eq. 1 can be taken as this unique direction. Shielding tensors, however, need not have any axial symmetry. As a general second rank tensor, σ can be decomposed into a sum of tensors of rank 0, 1, and 2:

$$\sigma = \sigma^{(0)} + \sigma^{(1)} + \sigma^{(2)}$$

Here $\sigma^{(0)}$ is the unit matrix (tensor) multiplied by the isotropic shielding, which is $(\sigma_{xx} + \sigma_{yy} + \sigma_{zz})/3$; this is a scalar quantity, independent of orientation. The rank 1 component $\sigma^{(1)}$ is the antisymmetric component of the full tensor:

$$\sigma^{(1)} \equiv (\sigma - \sigma^T)/2 \tag{5}$$

and the rank 2 tensor is the (traceless) orientation-dependent part of the symmetric component:

$$\sigma^{(2)} \equiv (\sigma + \sigma^T)/2 - \sigma^{(0)} \tag{6}$$

If we rotate the coordinate system to a frame where $\sigma^{(2)}$ is diagonal (which can always be achieved for a real symmetric tensor), then we can write:

$$\begin{aligned}\sigma^{(2)} &= \begin{bmatrix} \sigma_{11}-\sigma_{iso} & 0 & 0 \\ 0 & \sigma_{22}-\sigma_{iso} & 0 \\ 0 & 0 & \sigma_{33}-\sigma_{iso} \end{bmatrix} \\ &= \frac{1}{3}\Delta\sigma_1 \begin{bmatrix} 2 & 0 & 0 \\ 0 & -1 & 0 \\ 0 & 0 & -1 \end{bmatrix} + \frac{1}{3}\Delta\sigma_2 \begin{bmatrix} -1 & 0 & 0 \\ 0 & 2 & 0 \\ 0 & 0 & -1 \end{bmatrix}\end{aligned} \tag{7}$$

Here $\Delta\sigma_1 = \sigma_{11} - \sigma_{33}$, and $\Delta\sigma_2 = \sigma_{22} - \sigma_{33}$. The final line decomposes a general non-axial symmetric tensor into two axially symmetric parts, which can always be done. Note that the two tensors in the final line of Eq. 7 have values of $\sigma_n - \sigma_\perp$ of $\Delta\sigma_1$ and $\Delta\sigma_2$, respectively. We can treat the nitrogen CSA tensor as approximately axially symmetric, so that $\Delta\sigma_1 \equiv \Delta\sigma$ and $\Delta\sigma_2 = 0$. For the carbonyl carbon, however, the tensor is very rhombic, and both tensors (plus the cross correlations between them) must be considered to understand the relaxation process.

Normal mode analysis

Normal mode vibrational analysis is a standard topic (Goldstein 1980), and only an outline is given here. The basic idea is to expand the potential function $V(\mathbf{x})$ in a Taylor series expansion about some point $\mathbf{x}_0$:

$$V(\mathbf{x}) = V(\mathbf{x}_o) + \mathbf{g}\cdot(\mathbf{x}-\mathbf{x}_0) + \frac{1}{2}(\mathbf{x}-\mathbf{x}_0)\cdot\mathbf{F}\cdot(\mathbf{x}-\mathbf{x}_0) \tag{8}$$

If the gradient $\mathbf{g}$ of the potential vanishes at this point and one ignores third and higher-order derivatives, it is straightforward to show that the dynamics of the system can be described in terms of the normal mode directions and frequencies $\mathbf{Q}_k, \omega_k$, which satisfy:

$$\begin{aligned}&\mathbf{M}^{-1/2}\,\mathbf{F}\mathbf{M}^{-1/2}\,\mathbf{Q}_k = \omega_k^2\mathbf{Q}_k \\ &\mathbf{Q}_k\cdot\mathbf{Q}_j = \delta_{kj}\end{aligned} \tag{9}$$

In Cartesian coordinates, the matrix **M** contains atomic masses on its diagonal, and the Hessian matrix **F** contains the second derivatives of the potential energy evaluated at $\mathbf{x}_0$. The (classical) time evolution of the system is then:

$$x_i(t) = x_i(0) + 2^{1/2} \sum_k Q_{ik} m_i^{-1/2} \sigma_k \cos(\omega_k t + \delta_k) \qquad (10)$$

where σ_k is an amplitude, ω_k the angular frequency and δ_k the phase of the kth normal mode of motion. The phases and amplitudes depend upon the positions and velocities at time $t = 0$. The thermal averages of the second moments σ_k^2 of the amplitude distributions can be calculated for both classical and quantum statistics:

$$\sigma_{k,class}^2 = \frac{kT}{\omega_k^2}; \quad \sigma_{nk,qm}^2 = \frac{h}{4\pi\omega_k} \coth \frac{h\omega_k}{4\pi kT} \qquad (11)$$

where h and k are the Planck and Boltzmann constants. The two statistics coincide in the limits of low frequency or high temperature. For biomolecules, the most important difference is generally that higher frequency modes have little amplitude in classical statistics but have non-negligible zero-point motion in quantum statistics. Harmonic models thus provide one of the few practical ways for including quantum effects in biomolecular simulations.

Averages over the motion represented by normal modes are often carried out by Taylor-series expansions about $\mathbf{x}_0$ for each normal mode (Woodford and Harbison 2006), but for the present purposes, it is more convenient to randomly sample points from a thermal distribution:

$$\mathbf{x}^{(n)} = \mathbf{x}_0 + \sum_k s_k^{(n)} \mathbf{M}^{-1/2} \mathbf{Q}_k \qquad (12)$$

where $s_k^{(n)}$ is a pseudo-random number drawn from a Gaussian distribution with mean zero and variance σ_k^2. A quantum chemistry calculation can then be done at each point $\mathbf{x}^{(n)}$ and the results averaged (using Eq. 3) to yield the required averages over vibrational motion.

We applied this model to two model peptide systems, N-methylacetamide (NMA), and NMA_3, where the central peptide unit was hydrogen bonded on each side to another peptide model, as shown in Fig. 1, left. The geometries were minimized and normal modes calculated using the B3LYP density functional formalism and a 6-31G** basis set. Then 100 snapshots were obtained using Eq. 12 with quantum statistics at $T = 0$. For each snapshot, chemical shielding tensors were computed using a GIAO method, again with the B3LYP functional, but now with cc-pVTZ and cc-pVQZ basis sets. These were extrapolated to an approximate complete basis set (CBS) limit using a two-point extrapolation procedure we derived earlier:

$$\sigma(CBS) = -0.730\sigma(cc-pVTZ) + 1.730\sigma(cc-pVQZ) \qquad (13)$$

We have shown in previous work that such a CBS density functional approach gives shielding tensors for model peptides that are in reasonable agreement both with experiment (as best one can tell) and with CBS extrapolations from correlated wavefunctions at the MP2 level (Moon and Case 2006). There are certainly remaining limitations in this approach, both in representing correlation effects on shielding, and describing environmental effects such as hydrogen bonding, but the general trends reported here are expected to be reliable.

Path integral molecular dynamics

The equilibrium properties of a quantum system can also be approached by path-integral methods (Berne and Thirumalai 1986). This approach exploits an isomorphism between the quantum Boltzmann distribution (which is what we are looking for) and a classical system with P copies of each atom; in the classical system, the copies of each atom are connected by artificial spring forces, and the forces between atoms are reduced by a factor $1/P$. The classical system can then be simulated by conventional methods such as Monte Carlo or molecular dynamics methods. As the number of copies grows, the partition function of the classical system approaches the quantum limit. We have recently implemented path-integral molecular dynamics (PIMD) methods into the Amber simulation programs (Case et al. 2005; Paesani et al. 2006). Each of the

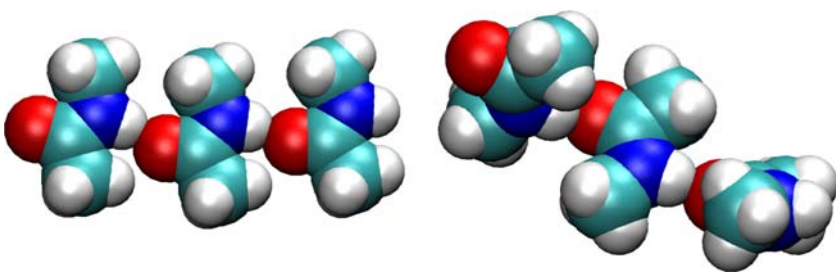

Fig. 1 *N*-methylacetamide trimer. Left: DFT-optimized structure for normal mode calculations; right: one snapshot of the fragment constructed from Phe30 in the PIMD simulation

P ''beads'' is simulated on a separate thread, and the springs are implemented via interprocess communication. A normal mode expansion in the bead coordinates is used to mitigate the stiffness of the dynamics between beads. Further details of the implementation are given by (Paesani et al. 2006).

We carried out a PIMD simulation of fragment B3 of protein G (''GB3'') using the Amber ff99sb force field for the protein (Hornak et al. 2006) and the q-SPCfw model for water (Paesani et al. 2006). (This is a preliminary simulation, since the water force field has been optimized for PIMD simulations but the protein force field has not.) After a classical equilibration, starting from the 1P7E pdb structure, the system was expanded to $P = 24$ beads, and 1 ns of normal-mode PIMD simulation was carried out with a time step of 0.5 fs. The temperature was regulated at 300 K with Nose-Hoover chains, and other details are as described by (Paesani et al. 2006). For this time period, the system was very stable, moving to structures with an RMS backbone deviation of about 0.7 Å from the starting structure, and maintaining all of the backbone secondary structure. Further analysis of this simulation will be given elsewhere.

Since we are primarily interested in local vibrational motion, we chose to analyze two residues, Phe30 and Phe52, that are in regular regions of the secondary structure of GB3: Phe30 is in the central helix, and Phe52 is part of the β sheet; both have low backbone mobility as measured by ^{15}N relaxation analysis (Hall and Fushman 2003). In order to minimize the effects of overall tumbling, and of other slow internal motions that might be present, we sampled points over a short (32 fs) period, starting (arbitrarily) at 1.025 ns. The structures we used for analysis were each of the 24 beads at four (real) time points separated by 8 fs, for a total of 96 structures. Test calculations (not shown) indicated that going to longer time periods (out to 100 fs) did not significantly alter the spread of structures being sampled. The sampling period represents a compromise between having enough time (and beads) to sample local vibrational motions, without having contamination by slower processes of such as overall rotational diffusion.

The 96 structures chosen in this fashion were then converted to model systems by extracting the $C\alpha^{i-1}$, C'^{i-1}, O^{i-1}, N^i, H^i, and $C\alpha^i$ atoms, for $i = 30$ or 52, along with the corresponding atoms of two peptide groups to which Phe30 or Phe52 are hydrogen bonded. Hydrogens were added with standard geometries to the Cα atoms, so that the fragment system was $(NMA)_3$ (see the right side of Fig. 1). These fragments were then subjected to the same analysis as described above for the normal mode analysis. That is shielding calculations were carried out using B3LYP and the cc-pVTZ and cc-pVQZ basis sets, the results were extrapolated to the complete basis limit, and the results averaged using Eq. 3.

Results

The general behavior of shielding tensors for atoms in a peptide group is well-understood (Sitkoff and Case 1998), and is illustrated in Fig. 2. For nitrogen, σ_{11} is roughly along the N–H bond, but displaced from it by about 20° as shown. The tensor is roughly axial about the σ_{11} direction, although rhombic components can be important for quantitative analysis. In our $(NMA)_3$ calculations, the average shieldings in the principal axis frame were 0.6, 147.7 and 186.0 ppm, giving a rhombicity parameter $\eta \equiv (\sigma_{22} - \sigma_{33})/(\sigma_{11} - \sigma_{iso})$ of 0.42 and a value of $\Delta\sigma \equiv \sigma_{11} - (\sigma_{22} + \sigma_{33})/2$ of –166.3 ppm. For *isotropic* motion, the effect of rhombicity is to increase $\Delta\sigma$ by a factor of $(1 + \eta^2/3)^{1/2}$, which is an increase of 3%. For anisotropic motion, the results will be somewhat different, but quite high precision data would be required to detect the effects of non-axial symmetry in NMR relaxation.

The carbonyl carbon tensor, on the other hand, is very non-axial. Average values from the $(NMA)_3$ model are –92.8, –17.7 and 80.3 ppm, so that any assumption of an axial tensor makes little sense. In our analysis, we will separate the total shielding tensor into two axial components as in Eq. 7. Overall CSA relaxation is then viewed as auto-relaxation of the two axial tensors, plus a cross-correlation between them.

^{15}N order parameters

For ^{15}N relaxation, the principal results are given in Tables 1 and 2. The *relative* effects of vibrational averaging are shown in Table 1, where all of the correlation functions are normalized to unity at $t = 0$. While there are

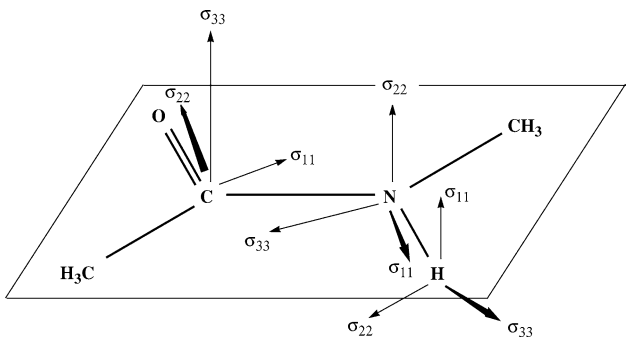

Fig. 2 Typical CSA tensor principal directions for peptides. The least-shielded component is denoted as σ_{11}, and the most-shielded component is σ_{33}. For each tensor, one of the components points in a direction very nearly perpendicular to the peptide plane

Table 1 ^{15}N CSA and N–H dipolar averages. For each cell, the average is normalized by dividing by the same quantity but with $t = 0$. The final column gives the product of columns 3 and 4, that is $\langle \omega_u(0) \cdot \omega_v(t) \rangle \cdot \langle P_2[\mathbf{u}(0) \cdot \mathbf{v}(t)] \rangle$. For dipolar interactions, ω is r^{-3}, where r is the N–H distance and **u** or **v** are unit vectors along the N–H bond direction. For the CSA interaction ω is $\Delta\sigma \equiv \sigma_{11} - (\sigma_{22} + \sigma_{33})/2$, and **u** or **v** are unit vectors along the σ_{11} direction (see Fig. 2)

interaction	*model*	$\langle P_2[\mathbf{u}(0) \cdot \mathbf{v}(t)] \rangle$	$\langle \omega_u(0) \cdot \omega_v(t) \rangle$	$\langle \omega_u(0) \cdot \omega_v(t) P_2[\mathbf{u}(0) \cdot \mathbf{v}(t)] \rangle$	3×4
dipolar	NMA	0.854	0.940	0.810	0.803
	NMA_3	0.861	0.959	0.829	0.826
	phe30	0.870	0.968	0.842	0.842
	phe52	0.897	0.963	0.862	0.864
CSA	NMA	0.972	0.956	0.930	0.929
	NMA_3	0.953	0.975	0.928	0.929
	phe30	0.971	0.979	0.951	0.951
	phe52	0.975	0.980	0.956	0.956
dipole-CSA	NMA	0.965	0.965	0.916	0.931
	NMA_3	0.940	0.988	0.921	0.929
	phe30	0.946	1.000	0.938	0.938
	phe52	0.955	0.989	0.935	0.944

Table 2 Effective ^{15}N CSA values. In the fourth column, **u** is along the N–H bond and **v** is along the σ_{11} direction of the ^{15}N CSA tensor. The angle β is defined such that $P_2(\cos\beta) = \langle P_2[\mathbf{u}(0) \cdot \mathbf{v}(0)] \rangle$

model	$\Delta\sigma_{av}$	$\Delta\sigma_{eff}$	$\langle P_2[\mathbf{u}(0) \cdot \mathbf{v}(0)] \rangle$	β
NMA	–137.2	–135.3	0.804	21.2°
NMA_3	–166.7	–162.6	0.797	21.6°
phe30	–160.3	–158.3	0.754	23.9°
phe52	–155.7	–153.7	0.779	22.6°

some differences between the four models considered here, a number of general trends are evident, and likely to be reliable. First, the effects of librational motions of the N–H bond are significant, even when just zero-point vibrational motion is considered. This can be seen in the third column of Table 1, where values of $\langle P_2[\mathbf{u}(0) \cdot \mathbf{v}(t)] \rangle$, which is the conventional S^2 parameter in the Lipari-Szabo model free analysis, ranges from 0.85 to 0.90. In addition this angular (or librational) dependence, fluctuations in the magnitude of the bond length have the effect of further reducing the effective dipolar coupling between the amide nitrogen and its attached proton. A more complete analysis of these zero-point motions, including estimates of anharmonic motions that are not included here, has been given earlier (Case 1999).

The dipolar order parameters shown here roughly match those measured for secondary structure residues in small proteins. For example, the S^2 values fitted to ^{15}N relaxation data for GB3 (Hall and Fushman 2003) are 0.861 and 0.827 for Phe30 and Phe52, respectively, if the N–H bond length is taken to be 1.01 Å, which is the actual equilibrium value from MP2 quantum chemistry calculations (Case 1999). This indicates that the peptide groups of these and similar residues are actually quite rigidly held to the overall molecular frame, since a model that includes only zero-point librations (and no internal peptide group rotation) fits the observed data quite well. Since most N–H vectors in secondary structure regions in GB3 (and in many other small proteins) have relaxation rates close to those observed for Phe30 and Phe52 in GB3, it is reasonable to argue that only local vibrational motion is being seen in ^{15}N relaxation measurements for these peptides. This view is in agreement with results from recent molecular dynamics simulations which also show peptide motions that can be interpreted in the same way (Buck and Karplus 1999; Buck et al. 2006; Hornak et al. 2006).

A second key point from Table 1 is that the zero-point orientational averaging of the CSA tensor is much less pronounced than for the N–H dipolar interaction: orientational S^2 values for the σ_{11} direction of the nitrogen CSA tensor (third column of Table 1) range from 0.95 to 0.97, which are much closer to unity than are the corresponding dipolar averages. The shielding tensor is an electronic structure property, and its directionality appears to be more strongly influenced by the positions of the heavy atoms (and in particular, of the partial double bond between C′

and N) than it is to the position of the amide proton. Since the zero-point vibrational amplitude of the light hydrogen atom is greater than that of the heavier carbon and nitrogen atoms, fluctuations in the direction of the CSA tensor are found to be much smaller than those of the N–H bond direction. This behavior is in contrast to the implicit assumption, found in most analyses of peptide relaxation, that the S^2 value for dipolar and CSA relaxation ought to be about the same. (The practical consequences of this error are mitigated by the fact the CSA tensor itself is often taken as a fitting parameter; we discuss this more below).

As one might expect, the orientational averaging of the cross-correlated interaction between dipolar and CSA relaxation is intermediate between that of pure dipolar and pure CSA relaxation, as shown in the final four rows of Table 1. The cross-correlated values are always much closer to the CSA values than to the dipolar values.

All of these interactions involve averaging both of angles (the third column of Table 1) and magnitudes of the interactions. For dipolar interactions, it has been known for a long time that these fluctuations are almost uncorrelated, so that the final two columns are nearly equal (Brüschweiler 1992). This statistical independence is also very accurate for the CSA-related fluctuations, as can be seen in the Table. So, at least for these relatively small vibrational motions, one can consider the angle and magnitude fluctuations separately when analyzing CSA relaxation.

Effective CSA tensors

The vibrational averaging we are considering here occurs on a sub-picosecond time scale, and is invariably in the extreme narrowing regime for NMR relaxation. The exact time-dependence for relaxation then becomes irrelevant, and the effect of the motion is to multiply the spectral density function expected for a rigid body by an order parameter, S^2. This order parameter can be, and often is, incorporated into an ''effective'' value of the bond length or shielding anisotropy. For dipolar interactions, we can write:

$$\left[\frac{1}{r^6}\right]_{eff} \equiv \left\langle \frac{P_2[\mathbf{u}(0)\cdot\mathbf{u}(t)]}{r^3(0)r^3(t)} \right\rangle_{vib} \tag{14}$$

Here $\mathbf{u}$ is a unit vector along the bond direction, and t is a time long compared to a vibrational time scale. Hence, a *rigid* molecule with a bond length of $r_{eff} \equiv \left[1/r^6\right]_{eff}^{-1/6}$ would have the same relaxation behavior as the actual system that includes the vibrational averaging. In a similar fashion, we can define an effective CSA tensor for pure CSA relaxation:

$$[\Delta\sigma]_{eff} \equiv \left[\langle \Delta\sigma(0)\Delta\sigma(t)P_2[\mathbf{u}(0)\cdot\mathbf{u}(t)]\rangle_{vib}\right]^{1/2} \tag{15}$$

This state of affairs for dipolar relaxation has been recognized for many years (Henry and Szabo 1985; Case 1999), and it is quite common for analyses of experimental relaxation behavior to approximately incorporate fast vibrational effects (including zero-point motion) into an effective bond length that is slightly longer than the actual equilibrium bond length. Estimates of these effective bond lengths can be derived from experiment (Ottiger and Bax 1998), or from quantum chemistry calculations much like those considered here (Case 1999). The two estimates are in quite good agreement, although both anharmonic effects and solvation corrections are required in a careful analysis. (For historical reasons, many analyses of ^{15}N relaxation in the literature use an effective bond length for the amide N–H bond of 1.02 Å. This is intermediate between the equilibrium bond length, which is about 1.01 Å, and a value of 1.04 Å that reflects local vibrational motion (Ottiger and Bax 1998; Case 1999)).

Our analysis now allows us to estimate the effective CSA tensors as defined in Eq. 15; these are listed in Table 2. The key general point here is that the effective tensor differs from the average tensor (*i.e.* the average of the values computed for each snapshot) by only 1.2–2.5%. This is a consequence of the high order parameters seen in Table 1. (Remember that $[\Delta\sigma]_{eff}$ is squared in expressions for pure CSA relaxation.) The actual values differ a lot in the four models we consider: NMA in vacuum has no hydrogen bond partners, and it is known that the effect of hydrogen bonding is to significantly increase $\Delta\sigma$. Hence we do not expect (or find) the NMA monomer results to be near to the tensors seen in proteins, which almost invariably have hydrogen bonding partners. The remaining three models have hydrogen bonding interactions, and consequently, more negative values of $\Delta\sigma$. The results from the PIMD simulation have the potential advantage of being extracted from a simulation of a real protein in water, but they have the disadvantage that the local geometries are determined by the molecular mechanics force field, which is known to have inaccuracies in both equilibrium geometries and in the extent of fluctuations about equilibrium (Mannfors et al. 2003). The local geometries and fluctuations given by the DFT results on $(NMA)_3$ are probably the more accurate in this respect, but here the hydrogen bonds are energetically optimized in a way that might not be possible in the context of an entire polypeptide chain. Overall, this means that the differences of ~10 ppm among the last three rows of Table 2 reflect real uncertainties in our models. One should also bear in mind that results for $\Delta\sigma$ in NMA vary by nearly 10 ppm depending on what density functional or correlation model is used, even at the

CBS limit (Moon and Case 2006). All of these factors limit the conclusions that can be drawn from the absolute CSA values (or effective values) reported here. Nevertheless, we expect our estimates of order parameters, which are a relative measure of motion, to be reliable.

It is worth noting that the individual tensors that go into the vibrational average have a lot of variability. Figure 3 shows histograms for the CSA in the snapshots used for NMA_3 and for the GB3 simulation. The standard deviation about the mean is 27 ppm for NMA_3 and 23 ppm for residue 30 in GB3. This implies that small changes in the geometry can have a significant impact on the shielding tensor, and suggests that it may be very difficult to find a single structure that is representative of the ensemble. For example, for NMA and NMA_3 we know the equilibrium structure (about which the normal mode expansion was made). The ^{15}N CSA for this average structure is –148.1 for NMA and –168.5 ppm for NMA_3; the latter is close to the vibrational average of –166.7 ppm (Table 2) but the former value is significantly different from the vibrational average of –137.2 ppm. Hence, simply computing a shielding tensor for an optimized structure may not always be sufficient to represent even the local vibrational averaging that is taking place. Further investigation of this question is ongoing. Finally, one should note that the variations shown in Fig. 3 have only a minor effect on relaxation: values of $\langle \omega_u(0) \cdot \omega_v(t) \rangle$ (fourth column of Table 1) vary between 0.96 and 0.98.

^{13}C relaxation

As mentioned above, CSA relaxation for the carbonyl carbon is more complex than for the amide nitrogen since the CSA tensor is very rhombic. We can express this as a sum of two axial tensors (Eq. 7), and look at the effects of averaging on each tensor, as well as on their cross-correlations. These are given in Table 3. Again, there are some differences for the various models, but the S^2 values (given in the last two columns of the table) range from 0.92 to 0.98. Fluctuations in the magnitude of $\sigma_1 = \sigma_{11} - \sigma_{33}$ are much smaller than those for $\sigma_2 = \sigma_{22} - \sigma_{33}$, as seen in column 4 of Table 3. This is in accord with a model that σ_{22} varies more strongly with conformation than does either σ_{11} or σ_{33} (Markwick and Sattler 2004; Loth et al. 2005). It should be noted, however, that the dependence of the carbonyl shielding tensor on environment in proteins is still under active study (see, e.g. (Burton and Tjandra 2007)), and variations over vibrational motion need not necessarily reflect variations of the average from one residue to another.

As with the amide nitrogen tensor, we can express the effects of local vibrational averaging in terms of an effective CSA tensor, and these values are collected in Table 4. As one would expect from the high values of S^2 shown in Table 3, the difference between average and effective tensors is quite small; remember that tensor is scaled according to the square root of S^2, that is, by 1–3% for values of S^2 between 0.98 and 0.94, as found here. Hydrogen bonding is an important contributor to the carbonyl CSA tensor, especially for $\Delta\sigma_2$. In the snapshot we chose, Phe30 (in the central helix) has well-formed hydrogen bonds, but the carbonyl of the Phe52 peptide (actually in residue 51) has only a weak hydrogen bond (average H...O length of 2.1 Å), even though it is in a region of regular secondary structure. Hence, the Phe30 results are close to that for the fully-hydrogen-bonded NMA_3 model, whereas those for Phe52 are close to those for NMA itself, which has no hydrogen bonds.

Recently, Jordan et al. (2007) have carried out an analysis of motional effects on carbonyl carbon CSA values, using (classical) molecular dynamics simulations on calmodulin. They analyze internal fluctuations of 50 peptide planes (not including overall or local dynamical events involving the peptide plane as a whole,) and find a average value of S^2 of 0.93. This is comparable to the values found in Table 3, and the general conclusion is the same as ours:

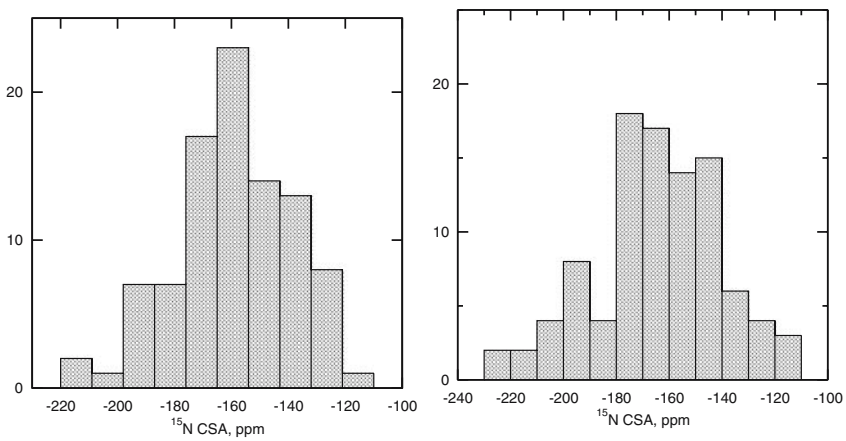

Fig. 3 Histogram of $\Delta\sigma$ values for Phe30 in GB3 (left) and for $(NMA)_3$ (right)

Table 3 ^{13}C CSA and Cα–C dipolar averages. For each cell, the average is normalized by dividing by the same quantity but with $t = 0$. For CSA-11, both **u** and **v** point along the σ_{11} direction and $\omega_u = \omega_v = \sigma_1$; for CSA-22, they both point along σ_{22} and $\omega_u = \omega_v = \sigma_2$; for CSA-12, **u** points along σ_{11} and **v** points along σ_{22}, with $\omega_u = \sigma_1$ and $\omega_v = \sigma_2$. The final column gives the product of columns 3 and 4, that is $\langle \omega_u(0) \cdot \omega_v(t) \rangle \cdot \langle P_2[\mathbf{u}(0) \cdot \mathbf{v}(t)] \rangle$

interaction	*model*	$\langle P_2[\mathbf{u}(0) \cdot \mathbf{v}(t)] \rangle$	$\langle \omega_u(0) \cdot \omega_v(t) \rangle$	$\langle \omega_u(0) \cdot \omega_v(t) P_2[\mathbf{u}(0) \cdot \mathbf{v}(t)] \rangle$	3×4
CSA-11	NMA	0.987	0.995	0.981	0.982
	NMA_3	0.943	0.995	0.938	0.938
	phe30	0.972	0.996	0.969	0.968
	phe52	0.990	0.992	0.982	0.982
CSA-22	NMA	0.986	0.956	0.943	0.943
	NMA_3	0.941	0.980	0.923	0.922
	phe30	0.969	0.986	0.956	0.955
	phe52	0.986	0.948	0.935	0.935
CSA-12	NMA	0.981	0.988	0.968	0.969
	NMA_3	0.954	0.994	0.948	0.948
	phe30	0.946	0.994	0.942	0.940
	phe52	0.984	0.981	0.965	0.965

Table 4 Effective ^{13}C CSA values. In the fourth column, **u** is along the N–C' bond, $\mathbf{v}_{11}$ is along the σ_{11} direction and $\mathbf{v}_{22}$ is along the σ_{22} of the ^{13}C CSA tensor. The angle β is defined such that $P_2(\cos\beta) = \langle P_2[\mathbf{u}(0) \cdot \mathbf{v}(0)] \rangle$

model	$\Delta\sigma_{1,av}$	$\Delta\sigma_{1,eff}$	$\Delta\sigma_{2,av}$	$\Delta\sigma_{2,eff}$	$\langle P_2[\mathbf{u}(0) \cdot \mathbf{v}_{11}(0)] \rangle$	$\langle P_2[\mathbf{u}(0) \cdot \mathbf{v}_{22}(0)] \rangle$	β_{11}	β_{22}
NMA	–173.7	–172.6	–70.2	–69.7	0.520	–0.023	34.5°	55.7°
NMA_3	–173.1	–168.1	–97.9	–95.0	0.451	0.046	37.2°	52.9°
Phe30	–175.8	–173.4	–95.7	–94.2	0.413	0.085	38.7°	51.4°
Phe52	–164.3	–163.5	–68.4	–68.0	0.422	0.075	38.4°	51.7°

local distortions of the peptide group should have only a small (1–3%) effect on the effective CSA tensor for carbonyl relaxation, even though the shielding tensor is actually quite sensitive to such distortions. This sensitivity, however, means that considerable care must be taken in comparing quantum chemistry calculations to experiment: it may be necessary to explicitly carry out motional averaging in the quantum calculations in order to obtain reliable results.

The final four columns of Table 4 give information about the orientation of the carbonyl shielding tensor relative to the peptide bond direction. This information is especially relevant for the analysis of cross-correlated relaxation between the CSA tensor and the C′–N dipolar interaction. The angle β_{11} is the effective angle between the σ_{11} direction and the C′–N bond direction. It is an ''effective'' value in the sense that a completely rigid peptide with this angle would exhibit the same cross-correlated relaxation as the actual (vibrating) peptide group of our models. This angle is in the range of 35–39°, which is in excellent agreement with results from solid-state NMR and from liquid-state relaxation studies (Sitkoff and Case 1998; Fischer et al. 1998; Loth et al. 2005; Jordan et al. 2007).

Discussion

Although CSA relaxation effects become increasingly important at high magnetic fields, relatively little is known about how shielding tensors vary with molecular conformation, nor about how these variations affect NMR relaxation. Here we use modern methods of computational chemistry to address one piece of the puzzle: what are the likely effects of local vibrational motion on the ^{15}N and ^{13}C′ tensors in peptide groups? Even this becomes a somewhat complex problem, since we need accurate calculations of electronic structures and reasonable models for nuclear motion that include zero-point vibrational effects. Uncertainties in how to best estimate these quantities leads to some variation in results, as seen in Tables 1–4. Nevertheless, some key conclusions can be drawn: fluctuations in the magnitude and directions of the ^{15}N CSA tensor are quite small, with squared order parameters in the

range 0.93–0.96; correspondingly, the effective shielding tensor (which would be used if vibrational averaging is ignored) is 2–4% smaller than the average tensor. The corrections for vibrational motion for CSA relaxation are much smaller than those needed for vibrational contributions to N–H dipolar relaxation. Squared order parameters for the carbonyl carbon CSA tensor are very similar (in the range of 0.92–0.95), with the σ_{22} component (which points roughly along the C=O bond direction) showing larger fluctuations than σ_{11} or σ_{33}.

Since the time scale for local vibrational motion is in the extreme narrowing limit for NMR relaxation, one can generally fold the effects of this motion into an effective tensor: the effective tensor shows the same relaxation behavior in a rigid system as the real tensor does for the vibrating system. Estimated values for these are given in Tables 2 and 4. These numbers can be compared to values extracted from various sorts of NMR experiments, but quantitative comparisons will require careful attention to the details of how the ''experimental'' tensors are determined. As an example, Kroenke et al. (1999) estimated the mean value of the ^{15}N CSA in ribonuclease H to be –172 ± 13 *ppm*, with a standard deviation in the site-to-site variation of 6 ppm. This analysis assumes an axially symmetric tensor, so is most directly comparable to $\Delta\sigma_{eff}(1+\eta^2/3)^{1/2}$ in the nomenclature of the present paper. Furthermore, the data extraction assumes that the spectral density $J(\omega)$ is the same for dipolar and CSA relaxation. If we take into account the fact the the dipole-dipole squared order parameter (S^2_{DD}) is different from the CSA-CSA value (S^2_{CSA}), we arrive at the following relation (see the Appendix):

$$\Delta\sigma_{eff}\left[1+\frac{\eta^2}{3}\right]^{1/2}=\Delta\sigma_{KRP}S_{DD} \tag{16}$$

Here $\Delta\sigma_{KRP}$ is the –172 ppm value extracted by Kroenke et al. (1999) from their experimental data. Setting S_{DD}; 0.94 and η; 0.42, a value of –172 ppm for $\Delta\sigma_{KRP}$ corresponds to a value of $\Delta\sigma_{eff}$ of 157 ppm. This is close to the values given in Table 2 for hydrogen-bonded models (the final three columns). Hence the effect of ignoring the rhombicity of the ^{15}N tensor (about a 3% reduction), and of assuming the same spectral density for dipolar and CSA relaxation (about a 6% reduction), combine to lower the fitted result by 15 ppm. This is roughly equal to the estimated standard deviation in the original paper. Hence, the elaborations given here are within the original statistical errors, but should become important as new measurements are made or as new types of data (such as from solid-state NMR) become available. We show in the Appendix that a similar re-interpretation can be made for other analyses of ^{15}N CSA values in proteins (Fushman and Cowburn 1998; Damberg et al. 2005; Hall and Fushman 2006). Given the limitations of the models used here, it is not possible to provide a convincing estimate of the possible errors in our estimated value for $\Delta\sigma_{eff}$, but all of the models predict that local vibrational motion should affect N–H dipolar relaxation to a much greater extent that it affects CSA relaxation. Further calculations, and careful analysis of both liquid and solid-state data will be required to know for sure exactly how big the difference is in representative protein environments.

In the end, the question of the ''best'' value to use for effective shielding tensors has no unique answer, and is similar to the question of assigning an effective bond length in relaxation calculations. A parameter like $\Delta\sigma_{KRP}$ is probably the simplest way to summarize the observed field dependence of relaxation rates. As long as one is consistent, this value can be plugged into calculations that assume a fixed value for $\Delta\sigma$. On the other hand, to make comparisons to theoretical calculations, or to compare fits to experiment where different assumptions and parameters might be used, it is useful to be able to back out estimates of the CSA tensor itself, or its vibrationally averaged effective value, $\Delta\sigma_{eff}$ (Eq. 15). Differences between these various estimates amount to only a few percent, with larger effects for nitrogen than for the carbonyl carbon, but they can be important if we are to extract structural or dynamic information from quantitative analyses of CSA tensors in proteins.

It is important to note that the motional effects described here are restricted to fast local vibrations. Peptide groups, particularly in loops and other mobile parts of a protein, can also undergo larger and slower internal motions, which we have not attempted to model here. For these larger motions, it is likely that the direction of the principal axes of the CSA tensor will follow the peptide plane, and the distinction between motion affecting dipolar relaxation and that affecting CSA relaxation will become less important. But these larger motions might also lead to fluctuations in the magnitude of $\Delta\sigma$ (as well as to its orientation); classical and path-integral dynamics simulations to investigate these larger motions are ongoing.

Acknowledgments This work was supported by NIH grant GM45811 and by ONR grant Utah/N00011-050100457. We thank Erik Zuiderweg, Art Palmer and Chad Rienstra for helpful conversations; and Jennifer Hall and David Fushman for providing details of their relaxation analysis for GB3.

Appendix

The procedure used by Kroenke et al. (1999) to estimate ^{15}N CSA values in proteins starts from expressions for

autorelaxation and crossrelaxation rate constants (their Eqs. 1 and 2):

$$\Gamma_{auto} = R_2 - 0.5R_1 - 0.454\sigma_{NH} = (3d^2 + 4c^2)J(0)/6 + R_{ex} \quad (17)$$

$$\Gamma_{cross} = (\eta_{xy}/\eta_z - 0.5)(R_1 - 1.249\sigma_{NH}) = (3d^2 + 4c^2)J(0)/6 \quad (18)$$

Here $d = \mathrm{h}\ \gamma_N\ \gamma_H < r_{NH}^{-3} >$ and $c = \omega_N\ \Delta\sigma\ /3^{1/2}$. The symbols have their standard meanings, as defined in the original paper. Assuming that R_{ex} is near zero, and that d is known, values of $J(0)$ and c can be determined from the field dependence of either Γ_{auto} or Γ_{cross}, since c is field dependent but $J(0)$ is not. If one fits the slope (m) and intercept (b) of a best-fit line of either Γ_{auto} or Γ_{cross} *vs.* ω_N^2, one can derive [Eq. 4 of Kroenke et al. (1999)]:

$$|\Delta\sigma_{KRP}| = (3d/2)(m/b)^{1/2} \quad (19)$$

For the residues analyzed, there was not a statistical difference between Γ_{auto} and Γ_{cross}, so a single slope could be used. The analysis excluded sites with chemical exchange broadening, or with high mobility (as monitored by the nitrogen-proton NOE). This is qualitatively similar to our selection here of two residues in well-formed secondary structure.

If we recognize that, in fact, $J(0)$ may be different for dipolar and CSA relaxation, we can make a model in which the principal differences occur from vibrational motion. Then:

$$J^{CSA}(\omega);\ S_{CSA}^2 J'(\omega);\ J^{DD}(\omega);\ S_{DD}^2 J'(\omega) \quad (20)$$

Here $J'(\omega)$ is the spectral density that would be present in the absence of fast vibrational motion, and this is assumed to be the same for either type of relaxation. The justification for this approximation is as follows: for large-scale rotations of the peptide group, the CSA tensor will follow the peptide plane orientation, as will the direction of the N–H bond. Hence, $J'(\omega)$ should be about the same for both types of interactions. For vibrational distortions, on the other hand, the distinction needs to be made, as is clear from Table 1. Replacing the single $J(0)$ in Eqs. 17 and 18 with separate values, as in Eq. 20, is equivalent to making the replacements

$$c \rightarrow cS_{CSA};\ d \rightarrow dS_{DD};\ J(0) \rightarrow J'(0) \quad (21)$$

Then, substituting this into Eqs. 17–19 and setting $\Delta\sigma_{eff} = S_{CSA}\ \Delta\sigma$ leads to Eq. 16 in the main text.

If one were to incorporate the effects of internal motion into an effective value of d (that is, of $< r_{NH}^{-3} >$), then S_{DD}^2 would be unity, and the fitting procedure used by Kroenke et al. (1999) would generate an effective value for $\Delta\sigma$ (aside from considerations of rhombicity). In practice, however, this analysis, along with many others, assumes a value of 1.02 Å for $< r^{-3} >^{-1/3}$, which captures some but not all of the vibrational reduction of the dipolar interaction strength (Case 1999). The remaining effects, which are mostly out-of-plane vibrations about the peptide nitrogen, also need to be considered. Experiments and calculations on small proteins or model peptides (Ottiger and Bax 1998; Case 1999) suggest that librational contributions would lead to an effective value of 1.041 Å for $< r^{-3} >^{-1/3}$; this corresponds to an additional contribution to S_{DD} of about a factor of $(1.02/1.041)^3; 0.94$. This estimate has been used in the main text to provide an updated estimate for $\Delta\sigma_{eff}$.

One could, of course, treat $\Delta\sigma_{KRP}$ of –172 ppm as yet another ''effective'' tensor, suitable for calculations where one assumes that the spectral densities are the same for the dipolar and CSA interactions, and that $< r_{NH}^{-3} >^{-1/3}$ is 1.02 Å. Or, if all local motion relevant to dipolar relaxation were subsumed into an effective bond length of 1.04–1.05 Å then the differences between S_{CSA} and S_{DD} (arising from slower motions) might be much smaller. But these are pretty strained definitions, and are not of much help in making comparisons to other experiments or to theoretical calculations. It is, after all, $\Delta\sigma$ itself which is the fundamental molecular parameter.

There are other methods of extracting nitrogen CSA tensors from liquid-state NMR relaxation data (Fushman and Cowburn 1998; Damberg et al. 2005; Hall and Fushman 2006), but these also assume a single spectral density and a known value of d that corresponds to $< r_{NH}^{-3} >$ of 1.02 Å. Hence, the same model can be used to allow for differences between dipolar and CSA vibrational order parameters. Note that this refitting has almost no effect on estimates of the site-to-site variability in ^{15}N tensors, which is still under active investigation.

References

Abragam A (1961) Principles of nuclear magnetism. Clarendon Press, Cambridge

Berne BJ, Thirumalai D (1986) On the simulation of quantum systems: path integral methods. Annu Rev Phys Chem 37: 401–424

Brüschweiler R (1992) Normal modes and NMR order parameters in proteins. J Am Chem Soc 114:5341–5344

Buck M, BouguetBonnet S, Pastor RW, MacKerell AD (2006) Importance of the CMAP Correction to the CHARMM22 Protein Force Field: dynamics of Hen Lysozyme. Biophys J 90:L36–L38

Buck M, Karplus M (1999) Internal and overall peptide group motion in proteins: molecular dynamics simulations for Lysozyme

compared with results from X-ray and NMR spectroscopy. J Am Chem Soc 121:9645–9658

Burton RA, Tjandra N (2007) Residue-specific 13C′ CSA tensor principal components for Ubiquitin: correlation between tensor components and hydrogen bonding. J Am Chem Soc 129: 1321–1326

Case DA (1999) Calculations of NMR dipolar coupling strengths in model peptides. J Biomol NMR 15:95–102

Case DA, Cheatham TE III, Darden T, Gohlke H, Luo R, Merz KM Jr, Onufriev A, Simmerling C, Wang B, Woods R (2005) The Amber biomolecular simulation programs. J Comput Chem 26:1668–1688

Cavanagh J, Fairbrother WJ, Palmer AG III, Rance M, Skelton NJ (2007) Protein NMR spectroscopy: principles and practice (2nd edn). Academic Press, Burlington, MA

Damberg P, Jarvet J, Graslund A (2005) Limited variations in 15N CSA magnitudes and orientations in Ubiquitin are revealed by joint analysis of longitudinal and transverse NMR relaxation. J Am Chem Soc 127:1995–2005

Fischer MW, Zeng L, Majumdar A, Zuiderweg ER (1998) Characterizing semilocal motions in proteins by NMR relaxation studies. Proc Natl Acad Sci USA 95:8016–8019

Fushman D, Cowburn D (1998) Model-independent analysis of ^{15}N chemical shift anisotropy from NMR relaxation data. Ubiquitin as a test example. J Am Chem Soc 120:7109–7110

Goldstein H (1980) Classical mechanics. Addison-Wesley, Reading, MA

Hall JB, Fushman D (2003) Characterization of the overall and local dynamics of a protein with intermediate rotational anisotropy: differentiating between conformational exchange and anisotropic diffusion in the B3 domain of protein G. J Biomol NMR 27:261–275

Hall JB, Fushman D (2006) Variability of the ^{15}N chemical shielding tensor in the B3 domain of protein G from ^{15}N relaxation measurements at several fields. Implications for backbone order parameters. J Am Chem Soc 128:7855–7870

Henry ER, Szabo A (1985) Influence of vibrational motion on solid state line shapes and NMR relaxation. J Chem Phys 82: 4753–4761

Hornak V, Abel R, Okur A, Strockbine B, Roitberg A, Simmerling C (2006) Comparison of multiple Amber force fields and development of improved protein backbone parameters. Proteins 3:712–725

Ishii Y, Terao T, Hayashi S (1997) Theory and simulation of vibrational effects on structural measurements by solid-state nuclear magnetic resonance. J Chem Phys 107:2760–2774

Jordan DM, Mills KM, Adricioaei I, Bhattacharya A, Palmo K, Zuiderweg ERP (2007) Parameterization of peptide ^{13}C carbonyl chemical shielding anisotropy in molecular dynamics simulations: effects of dynamics local distortions on ^{13}C carbonyl NMR relaxation, preprint

Kowalewski J, Mäler L (2006) Nuclear spin relaxation in liquids: theory, experiments, and applications. Taylor & Francis, New York

Kroenke CD, Rance M, Palmer AG III (1999) Variability of the ^{15}N chemical shift anisotropy in *Escherichia coli* ribonuclease H in solution. J Am Chem Soc 121:10119–10125

Lipari G, Szabo A (1982) Model-free approach to the interpretation of nuclear magnetic resonance relaxation in macromolecules. I. Theory and range of validity. J Am Chem Soc 104:4546–4559

Loth K, Pelupessy P, Bodenhausen G (2005) Chemical shift anisotropy tensors of carbonyl, nitrogen, and amide proton nuclei in proteins through cross-correlated relaxation in NMR spectroscopy. J Am Chem Soc 127:6062–6068

Mannfors BE, Mirkin NG, Palmo K, Krimm S (2003) Analysis of the pyramidalization of the peptide group nitrogen: implications for molecular mechanics energy functions. J Phys Chem A 107:1825–1832

Markwick PRL, Sattler M (2004) Site-specific variations of carbonyl chemical shift anisotropies in proteins. J Am Chem Soc 126:11424–11425

Moon S, Case DA (2006) A comparison of quantum chemical models for calculating NMR shielding parameters in peptides: mixed basis set and ONIOM methods combined with a complete basis set extrapolation. J Comput Chem 27:825–836

Nielsen PA, Norrby P-O, Liljefors T, Rega N, Barone V (2000) Quantum mechanical conformational analysis of beta-alanine zwitterion in aqueous solution. J Am Chem Soc 122:3151–3155

Ottiger M, Bax A (1998) Determination of relative N–HN, N–C′, and C alpha–H alpha effective bond lengths in a protein by NMR in a dilute liquid crystalline phase. J Am Chem Soc 120:12334–12341

Paesani F, Zhang W, Case DA, Cheatham TE, Voth GA (2006) An accurate and simple quantum model for liquid water. J Chem Phys 125:184507

Sitkoff D, Case DA (1998) Theories of chemical shift anisotropies in proteins and nucleic acids. Prog NMR Spectr 32:165–190

Tjandra N, Bax A (1997) Direct measurement of distances and angles in biomolecules by NMR in a dilute liquid crystalline medium. Science 278:1111–1114

Torchia DA, Szabo A (1982) Spin-lattice relaxation in solids. J Magn Reson 49:107–121

Tsui V, Zhu L, Huang TH, Wright PE, Case DA (2000) Assessment of zinc finger orientations by residual dipolar coupling constants. J Biomol NMR 16:9–21

Woodford JN, Harbison GS (2006) Effects of zero-point and thermal vibrational averaging on computed NMR properties of a model compound for purine nucleosides. J Chem Theory Comput 2:1464–1475